Matter

CellPress

Article

Ultrafast high-temperature sintering to avoid metal loss toward high-performance and scalable cermets

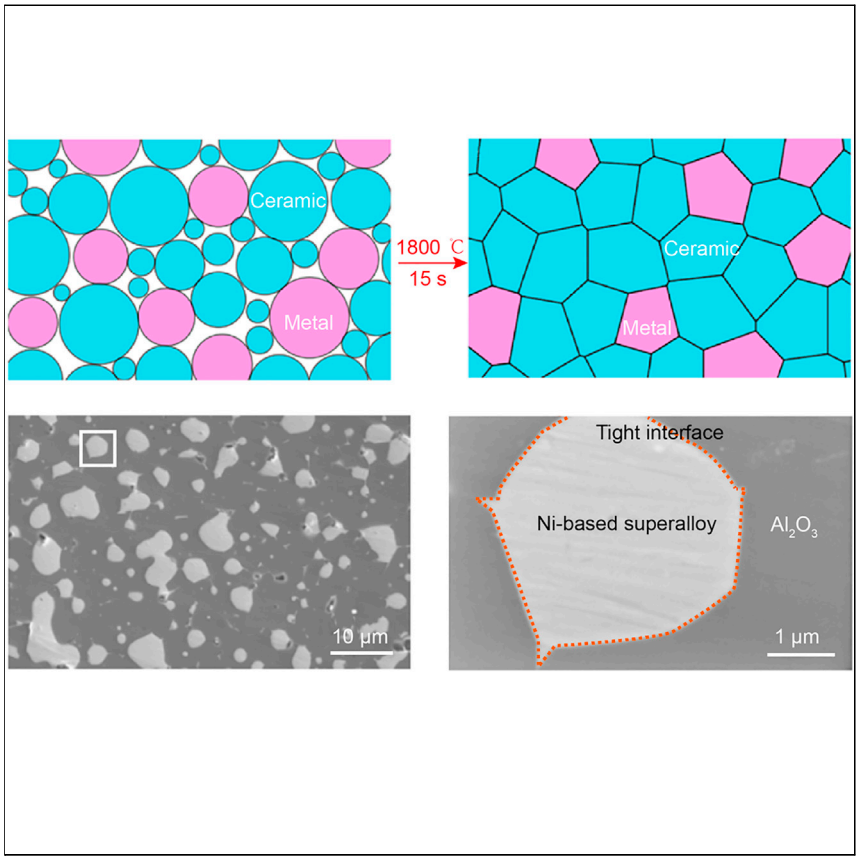

Cermet sintering faces many challenges, such as metal volatilization, grain coarsening, and poor wettability of metal with the ceramic phase. In this work, we apply an ultrafast high-temperature sintering (UHS) method to sinter high-quality cermets in only seconds. The high temperature leads to good wettability of metal with the ceramic phase, while the short sintering time limits the loss of metal components as well as accurately controlling the grain growth.

Miao Guo, Qi Dong, Hua Xie, ..., Wei Xiong, Ji-Cheng Zhao, Liangbing Hu

jczhao@umd.edu (J.-C.Z.)
binghu@umd.edu (L.H.)

Highlights

Cermets were achieved by an UHS method

Our UHS method can inhibit the metal volatilization for high material quality

Our UHS method can sinter a range of cermet compositions, shapes, and sizes

This approach potentially expands the application of cermets in various fields

Guo et al., Matter 5, 594–604
February 2, 2022
https://doi.org/10.1016/j.matt.2021.11.008

6 **Development**
Practical, real world, technological considerations and constraints

CellPress

Matter

Article

Ultrafast high-temperature sintering to avoid metal loss toward high-performance and scalable cermets

Miao Guo,[1,4] Qi Dong,[1,4] Hua Xie,[1] Chengwei Wang,[1] Yunhao Zhao,[2] Xizheng Wang,[1] Wei Zhong,[1] Zhihan Li,[1] Ruiliu Wang,[1] Yuankang Wang,[2] Liangyan Hao,[2] Shuaiming He,[1] Gang Chen,[1] Wei Xiong,[2] Ji-Cheng Zhao,[1,*] and Liangbing Hu[1,3,5,*]

SUMMARY

Cermets embrace the high hardness of a ceramic and the good ductility of a metal. Therefore, they potentially meet the ever-increasing demands of new materials for harsh environments in energy generation and conversion. However, cermet sintering faces many challenges, such as metal volatilization, grain coarsening, and poor wettability of the metal with the ceramic, which affect the microstructure and thus mechanical properties. Herein, we apply an ultrafast high-temperature sintering (UHS) method to sinter cermets at a high temperature in only seconds. The high temperature leads to good wettability of the metal with the ceramic, while the short sintering time limits the loss of metal components and accurately controls the grain growth. We demonstrate the UHS method using a model cermet composed of a Ni-based superalloy and aluminum oxide, where we obtain dense microstructure, minimal nickel loss, and uniform grain size. Owing to these merits, good mechanical properties and oxidation resistance are achieved.

INTRODUCTION

High-temperature materials are indispensable to many areas, such as gas turbines and jet engines.[1–5] Among a variety of candidate materials, cermets stand out as they embrace the merits of both metals and ceramics.[6–10] For example, the good ductility of the metallic phase often contributes to superior thermal shock resistance and good fracture toughness, which are required under harsh operating conditions for gas turbines but are challenging for conventional ceramics.[11–13] On the other hand, the high melting point of the ceramic component (typically >2,000°C) usually offers superior heat tolerance, high oxidation, and hot corrosion resistance, which often cannot be achieved using metals alone. Despite these features, sintering of cermets faces a number of challenges. The volatilization of the metal constituent and poor wettability of the metal with the ceramic make it difficult to achieve a highly dense microstructure. In addition, the conventional long sintering time often leads to uncontrolled grain coarsening, which degrades the mechanical performance of the sintered cermets.

To meet these challenges, we leverage a newly invented ultrafast high-temperature sintering (UHS) process[14,15] to sinter a range of cermets at high temperature (e.g., 1,800°C) in only seconds. Figures 1A and 1B demonstrate our UHS process from a green pellet (Figure 1A) made of ceramic and metal precursors to densified cermets (Figure 1B). The process is based on Joule heating of carbon materials

Progress and potential

Cermets (ceramic-metal composites) leverage the high hardness (and strength) of a ceramic and the good ductility of a metal to achieve a balance of properties that cannot be achieved by either constituent alone. Therefore, they potentially meet the ever-increasing demands of new materials for harsh environments in energy generation and conversion. However, cermet sintering faces many challenges, such as metal volatilization, grain coarsening, and poor wettability of metal with the ceramic phase, which affect the microstructure and thus the mechanical properties. In this study, we apply an ultrafast high-temperature sintering (UHS) method to sinter cermets at a high temperature in only seconds. Good mechanical properties and oxidation resistance are achieved. Our method can be extended to a range of cermet compositions, shapes, and sizes with high quality, potentially expanding the future development of cermets for various applications.

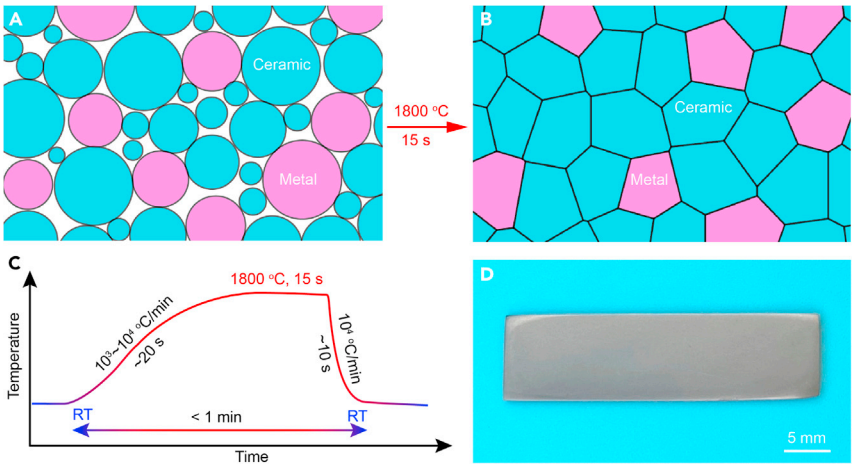

Figure 1. Our UHS approach for cermet sintering

(A and B) Schematic of our sintering process from a green pellet containing ceramic and metal precursor mixture to the sintered cermets.

(C) The temperature profile during the UHS process.

(D) The sintered cermet with a glossy surface after polishing with sand paper. Sample size: 34 × 9 × 1 mm.

that enables short heating durations (i.e., seconds versus hours by traditional sintering) because of the fast heating (10^3°C/min – 10^4°C/min) and cooling rates (up to 10^4°C/min) (Figure 1C). The high temperature contributes good metal wettability to the ceramic phase and fast densification of the cermet. Meanwhile, the short sintering duration (i.e., ~15 s of heating, ~45 s including ramping and cooling steps owing to the fast ramping and cooling rates) limits the metal volatilization and controls the grain growth, thereby achieving a highly dense microstructure with good mechanical properties. In comparison, it is challenging to reduce metal volatilization by conventional furnace sintering due to the low heating (e.g., <100°C/min) and cooling rates (e.g., <10°C/min),[16–18] which together result in long heating durations (Figure S1). In this case, using a lower temperature (e.g., 1,400°C) can reduce metal loss but is incapable of densifying the ceramic matrix (Figure S2), while using a higher temperature (e.g., 1,700°C) can improve wetting and densification but causes severe loss of volatile metallic substances (Figure S3).

We use UHS to sinter a model cermet system (i.e., a Ni-based superalloy [20 vol %] and Al_2O_3 [80 vol %]) as a proof-of-concept. Figure 1D displays a typical sintered cermet (dimensions: 34 × 9 × 1 mm) with a glossy surface after polishing. For conventional methods, the high temperature and long-term sintering caused severe loss of nickel component (5.75 wt %) due to the large melting temperature difference between the Ni-based superalloy (~1,500°C) and Al_2O_3 (~2,000°C), leading to pores and defects (relative density is only 76.4%). In comparison, our UHS can achieve highly dense microstructure (relative density is 94.3%), negligible loss of nickel component (1.80 wt %), and uniform grain sizes (~2–6 μm). Owing to the superior materials quality, the cermet produced by UHS exhibits excellent mechanical properties and high-temperature stability (*vide infra*). Our method is not only scalable for large sample sizes (e.g., 34 × 9 × 1 mm) but also flexible in shapes (e.g., star, heart, and bone shapes) by adjusting the carbon heater. In addition, the UHS method is generally applicable to a range of cermet compositions, where we demonstrate high-quality Ni-based superalloy with ZrO_2 and the Ni-based

[1]Department of Materials Science and Engineering, University of Maryland, College Park, MD 20742, USA

[2]Physical Metallurgy and Materials Design Laboratory, Department of Mechanical Engineering and Materials Science, University of Pittsburgh, Pittsburgh, PA 15261, USA

[3]Center for Materials Innovation, University of Maryland, College Park, MD 20742, USA

[4]These authors contributed equally

[5]Lead contact

*Correspondence: jczhao@umd.edu (J.-C.Z.), binghu@umd.edu (L.H.)

https://doi.org/10.1016/j.matt.2021.11.008

superalloy with yttria-stabilized zirconia (YSZ). This study opens up a new door toward ultrafast, scalable, and high-quality cermet sintering.

RESULTS AND DISCUSSION

We demonstrate this approach using a model cermet system composed of a Ni-based superalloy as the metal phase and aluminum oxide (Al_2O_3) as the ceramic phase. In this composition, the Ni-based superalloy provides toughening and reinforcing effects on the ceramic matrix,[19] while α-Al_2O_3 offers good corrosion and oxidation resistance as well as high hardness to the whole material.[20] In a typical sintering process, we sandwich a pressed green pellet between two Joule-heated carbon felt strips (Figures 2A, S4A, and S4B), whose temperature can be controlled by tuning the electrical input. The temperature of the carbon heater was measured using a high-speed camera (Figures 2A and S4C), the result of which showed a positive correlation with the input power (Figure S4D). During sintering, the temperature was quickly ramped to 1,800°C in 20 s, then held constant for ~15 s, followed by fast quenching to room temperature in 10 s by turning off the electrical power. After sintering, the pellet exhibits 27% shrinkage (from 10 to 7.3 mm in diameter) and a metallic luster upon polishing (Figure 2B).

We used scanning electron microscopy (SEM) to characterize the cross-section of the sintered pellet and observed a highly dense and uniform microstructure (Figures 2C and 2D). SEM images at higher magnifications confirm the well-sintered Al_2O_3 phase and a tight interface between the Ni-based superalloy and Al_2O_3 (Figures 2E and 2F). We used energy-dispersive X-ray spectroscopy (EDS) to map the distribution of Ni, Al, and O, where minimal cross-diffusion between the metal and Al_2O_3 phase can be detected (Figure 2G). The sintered cermet was further characterized by X-ray diffraction (XRD), the diffraction pattern of which agrees with a combination of Ni-based superalloy and α-Al_2O_3, with only a minor impurity peak corresponding to $NiCr_2O_4$ (Figure 2H), which was formed as the result of NiO interacting with Cr_2O_3 from the Ni-based superalloy. Note that upon the ultrafast sintering, the Al_2O_3 precursor (Figure S5) transformed to a stable, high-strength, corrosion-resistant, and oxidation-resistant α-Al_2O_3 phase, which is beneficial to the overall properties of the cermet. These results confirm the successful formation of cermet composed of a Ni-based superalloy and Al_2O_3 with high materials quality using our UHS approach.

To understand the detailed sintering process and the evolution of microstructure, we conducted ultrafast sintering by varying the sintering temperature and duration with the same cermet composition (i.e., Ni-based superalloy [20 vol %] and Al_2O_3 [80 vol %]). Microscopically, we find that low sintering temperatures (e.g., 1,600°C, 15 s) and shorter sintering durations (e.g., 5 s, 1,800°C) generally lead to poor densification (Figures 3A and 3B). Macroscopically, the under-sintered pellets show relatively lighter color and less shrinkage (from 10 to 7.8 mm in diameter) compared with the optimal conditions (*vide infra*). On the other hand, high sintering temperatures (e.g., 2,300°C, 15 s) and long sintering durations (e.g., 25 s, 1,800°C) result in over-sintering of the cermet, creating a porous microstructure due to the volatilization of the metal components (Figures 3C and 3D). The over-sintered pellets also display some extent of deformation and inhomogeneous colors. In comparison, optimal sintering was achieved at 1,800°C for ~15 s. Under such conditions, the sintered pellet exhibits uniform metallic luster and highly dense microstructure (Figures 3E and S6).

The effect of sintering temperature and sintering duration was further studied. Figure S6 compares the cermet pellets sintered at different temperatures (i.e., 1,600°C, 1,800°C, and 2,300°C) for the same sintering time (~15 s). The cermet pellets

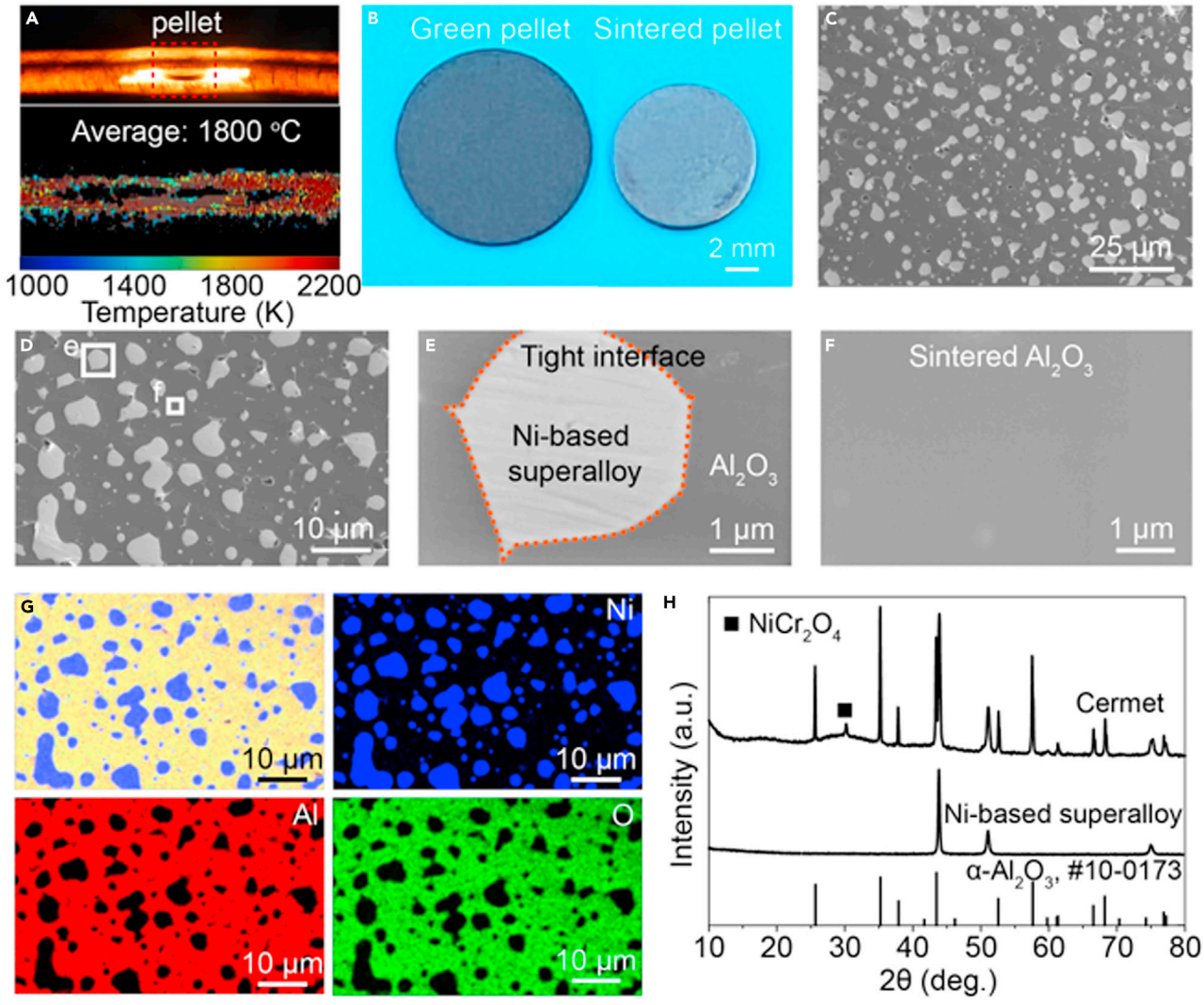

Figure 2. Applying the UHS method on a model cermet system composed of a Ni-based superalloy and Al_2O_3

(A) Pellet sandwiched between two Joule-heated carbon felt strips during sintering and the corresponding temperature mapping.

(B) Photo of the green and sintered cermet pellets.

(C) Low-magnification cross-section SEM image of the sintered cermet.

(D) High-magnification cross-section SEM image of the sintered cermet.

(E) SEM image of the metal/ceramic interface, showing the tight interfaces.

(F) SEM image of the Al_2O_3 phase, showing the highly dense microstructure.

(G) EDS mapping of Ni, Al, and O.

(H) XRD pattern of sintered cermet as compared with that of the original Ni-based superalloy powder and the standard diffraction pattern of α-Al_2O_3.

sintered at a low temperature (1,600°C) do not have sufficient densification of the ceramic matrix, leaving a large amount of pores in the pellet. With the increase of temperature to 1,800°C, the metal phase aggregates into large and regular grains, while the ceramic phase starts to densify and form an intimate interface with the metal phase. When the temperature further increases to 2,300°C, volatilization of the metal phase occurs, the rate of which is much faster than the densification of the ceramic phase. Therefore, a large amount of pores form during sintering, with sizes larger than those from the sintered pellets at low temperatures. The effect of the sintering duration is demonstrated in Figure S7, where the cermet exhibits gradually densified microstructure from 5 to 15 s at 1,800°C. The cermet exhibited similar

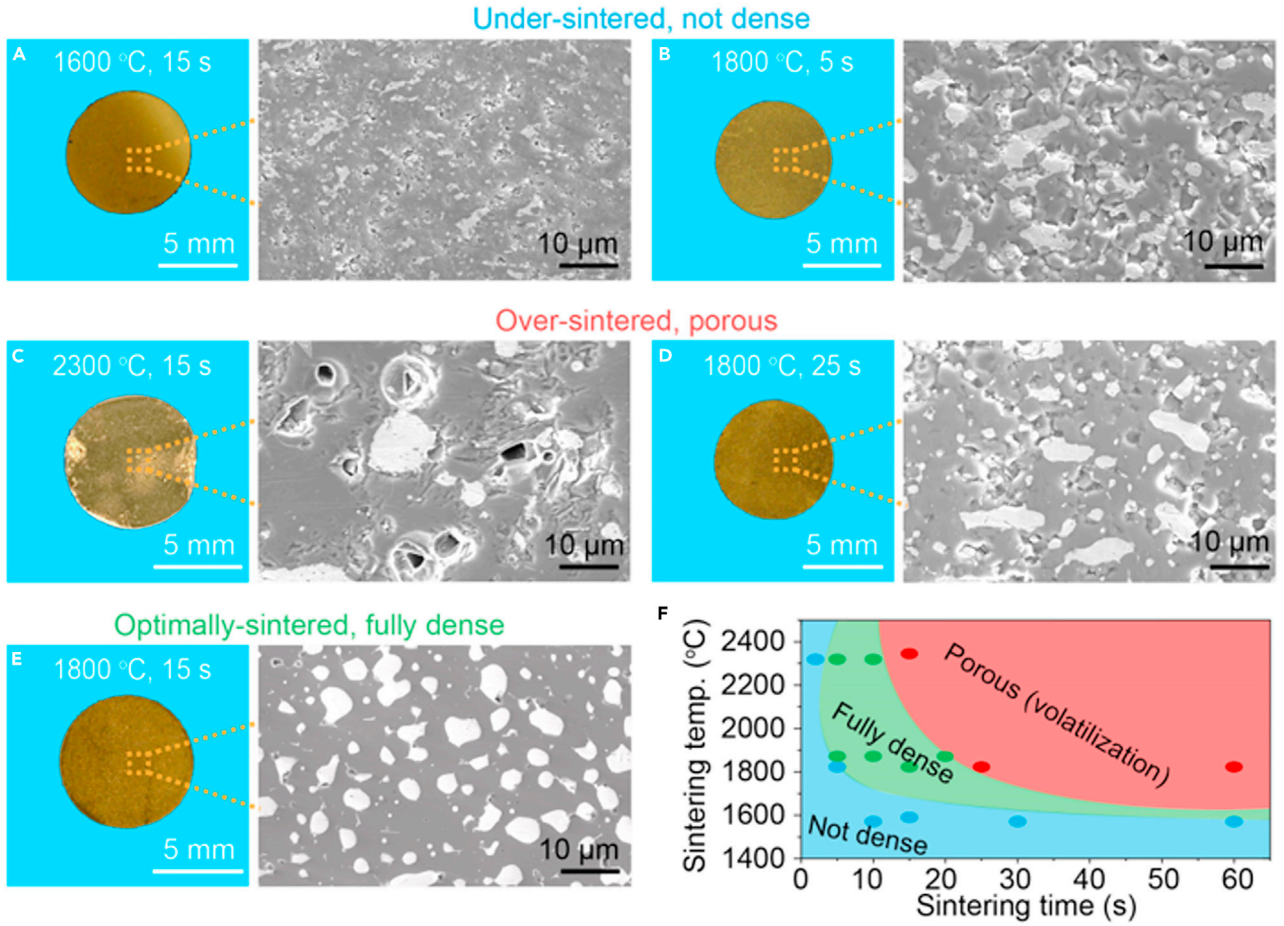

Figure 3. Time-temperature-transformation relationship of cermet sintered using UHS

(A and B) Photos and SEM images of the under-sintered cermet at 1,600°C for 15 s and 1,800°C for 5 s, respectively.

(C and D) Photos and SEM images of the over-sintered cermet at 2,300°C for 15 s and 1,800°C for 25 s, respectively.

(E) Photo and SEM image of the cermet sintered at the optimal condition of 1,800°C for 15 s.

(F) Time-temperature-transformation diagram of the cermet composed of the Ni-based superalloy and Al_2O_3 (volume ratio is 1:4).

dense microstructure at different positions after sintering 15 s (Figure S8), which proves the uniform temperature distribution in the cermet pellet. As heat is conducted through the carbon heater to the middle of the pellet, the area near the surface can be densified in 5 s while the middle area remains porous (Figure S9). When sintering at 1,800°C for 25 s, the long sintering duration results in the volatilization of the metal phase and thus a porous microstructure (Figures 3D and S7). Based on a series of sintering conditions, we construct the time-temperature-transformation diagram, which can be used to guide the cermet sintering process toward a desired microstructure (Figure 3F).

Other than the sintering temperature and duration, the mixing state of the precursor also plays an important role in the quality of the sintered cermet. We show that the optimal mixing of the precursor powders (e.g., by ball milling) is critical to achieve a dense microstructure; in contrast, a poor mixing quality can lead to a porous microstructure despite using the optimized sintering conditions (Figure S10). In addition, by comparing the pure Al_2O_3 and the Ni-based superalloy and Al_2O_3 cermet sintered in the same batch, we found that the addition of metal facilitates the

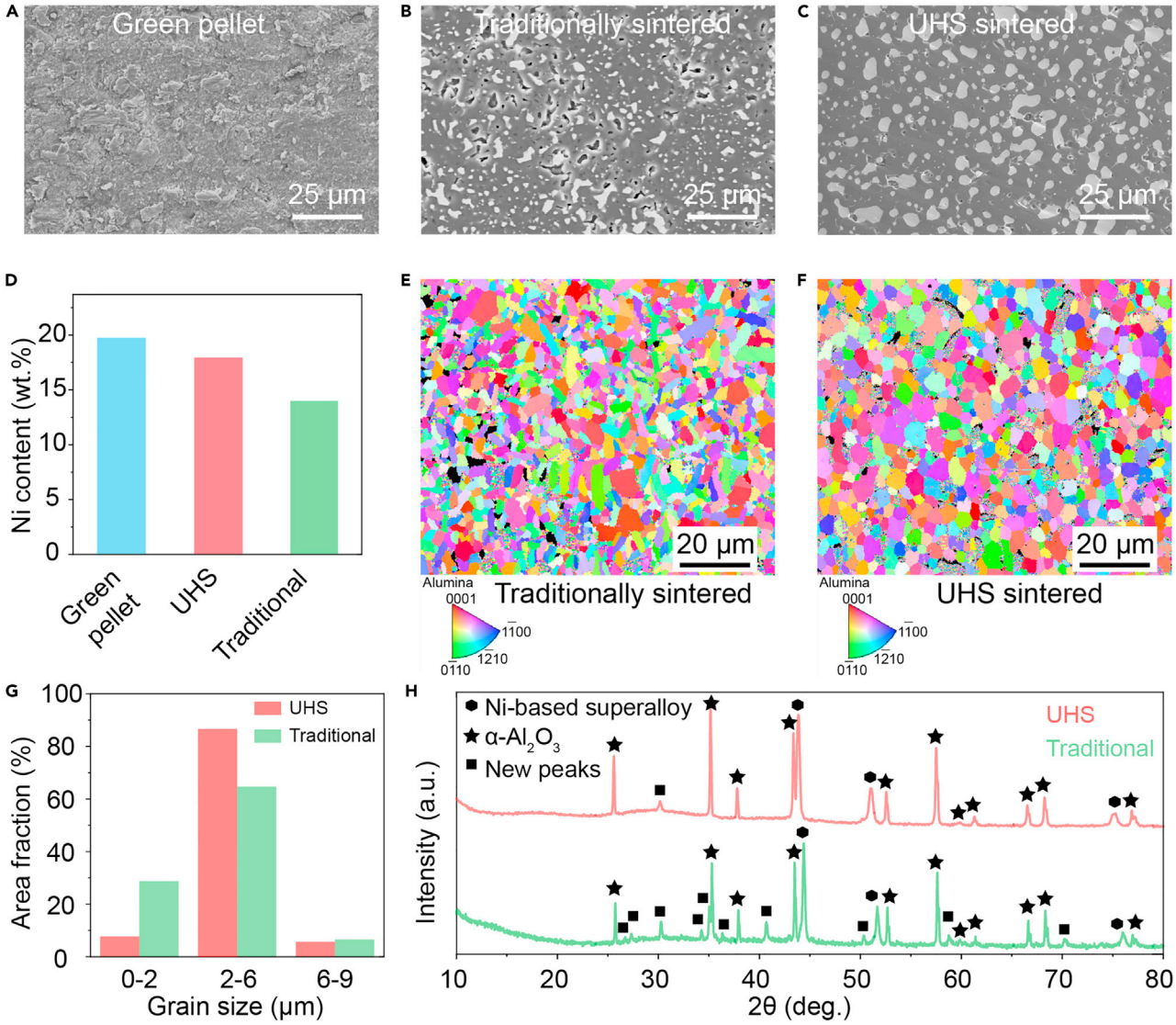

Figure 4. Comparison of the cermet sintered in a traditional furnace and with our UHS approach

(A) SEM image of the green pellet.

(B) SEM image of the pellet sintered using a traditional furnace.

(C) SEM image of the pellet sintered using our UHS method.

(D) Ni contents in the green pellet, the pellet sintered in a traditional furnace, and using our ultrafast method.

(E) EBSD map of the pellet sintered in a traditional furnace.

(F) EBSD map of the pellet sintered using our UHS approach.

(G) Grain size distribution of the cermet pellets sintered in a traditional furnace and by our UHS approach.

(H) XRD patterns of the cermet pellets sintered in a traditional furnace and using our UHS approach.

densification of the ceramic owing to the liquid-phase sintering mechanism (Figure S11).

Using this model system featuring a Ni-based superalloy and Al_2O_3, we compared the cermet quality by traditional sintering and our ultrafast sintering approach. Figures 4A–4C show the SEM images of the green pellet, the pellet sintered using a traditional furnace, and that using UHS, respectively. Compared with the furnace-sintered pellet where the sintering temperature and time were optimized to

minimize metal loss, the cermet obtained via UHS shows a denser microstructure. To quantify the density, we calculated the relative density of both UHS-sintered and traditionally sintered cermet pellets. Our UHS-sintered pellets have a much higher relative density of 94.3% than traditionally sintered pellets (76.4%). We measured the Ni contents in the green pellet, the pellet sintered using a traditional furnace, and that by our ultrafast method by inductively coupled plasma atomic emission spectroscopy. The Ni contents in the green pellet, UHS, and traditionally sintered pellets were 19.75 wt %, 17.95 wt %, and 14.00 wt %, respectively (Figure 4D). The cermet sintered using UHS exhibits much less loss of Ni (1.80 wt %) as compared with the furnace-sintered cermet (5.75 wt %). Electron backscatter diffraction (EBSD) maps for the cermet sintered using a traditional furnace and using UHS are shown in Figures 4E and 4F, respectively. The cermet sintered using UHS shows desirable uniform and equiaxial grains, while the grains of the furnace-sintered cermet have a large size variation. We calculated the grain size distribution based on EBSD maps (Figures 4G and S12). The cermet sintered using UHS has a narrow grain size range of ~2–6 μm, while that of the cermet sintered using the traditional method has a much wider distribution. We further conducted XRD on the cermets sintered using both UHS and a conventional furnace, where the former exhibits purer phase compositions and the latter shows more impurities that likely result from cross-diffusion and side reactions of different metallic atoms in the Ni-based superalloy due to the long sintering time (Figure 4H).

We characterized the mechanical properties of the sintered cermet using a range of methods. The three-point bending and compressive stress-strain curves of the cermet and bare Al_2O_3 sintered using UHS (Figures 5A and 5B) reveal that the addition of the Ni-based superalloy leads to toughening and reinforcing effects on the Al_2O_3 ceramic matrix. Notably, the cermet exhibits a bending strength of 368 $\pm$ 51 MPa and a compressive strength of 1,460 $\pm$ 24 MPa, which are much higher than those of Al_2O_3 (198 $\pm$ 5 MPa, 349 $\pm$ 50 MPa) (Figures 5C and 5D). In addition, the cermet shows uniform Vickers hardness in different regions (Figure S13), with an average hardness of 12.84 GPa (Figure 5E) and a fracture toughness of 5.28 MPa $m^{1/2}$. These mechanical properties of the cermet sintered using UHS are comparable with the literature reports based on similar compositions.[21–27] Owing to the desired quality of the sintered cermet, we achieve excellent oxidation resistance with a weight increase of 1.34 mg and a specific surface weight increase of only 1.30 mg cm^{-2} after 100 h at 1,100°C in air (Figure 5F).

As our method is based on Joule heating of carbon materials, it offers good scalability for larger sample dimensions through adjusting the size of the carbon heaters (Figure S14). In addition, as shown in Figures 5G–5I, our method can be used to sinter various shapes (e.g., bone, star, and heart) to accommodate different application requirements. Moreover, our method is capable of mass production, where we show batch sintering of multiple cermet pellets at the same time (Figure S15). Note that the UHS approach is not limited to the specific composition studied above. We further demonstrate two other cermet systems composed using the Ni-based superalloy and ZrO_2 (Figure S16) and the Ni-based superalloy and YSZ (Figure S17), both showing highly dense microstructures.

Conclusions

In conclusion, we demonstrate an ultrafast and general sintering approach for high-quality cermet manufacturing. The fast ramping to high temperatures induces rapid densification of both ceramic and metal phases, while the short sintering duration (~15 s) limits the volatilization of the metal component. Using a model cermet

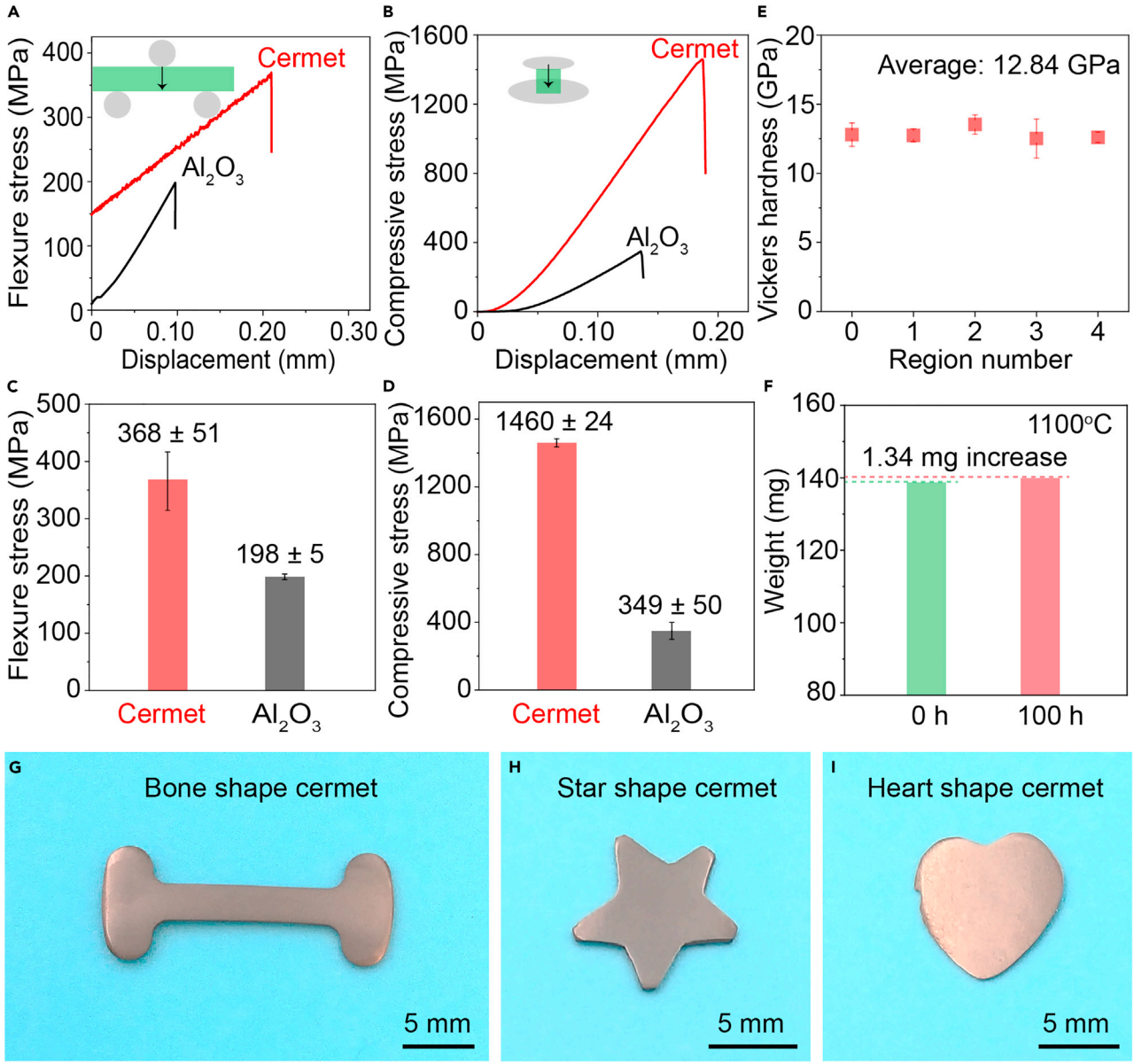

Figure 5. Superior performance and shape flexibility of cermets prepared by UHS

(A) The three-point bending stress-strain curves of cermet and Al_2O_3.

(B) Compressive stress-strain curves of cermet and Al_2O_3.

(C) The flexure stress of cermet and Al_2O_3. Error bars denote standard deviation.

(D) Compressive stress of cermet and Al_2O_3. Error bars denote standard deviation.

(E) Vickers hardness of cermet in different regions.

(F) Weight change of the sintered cermet before and after the high-temperature oxidation resistance test at 1,100°C for 100 h in air.

(G) Photo of a bone-shaped cermet.

(H) Photo of a star-shaped cermet.

(I) Photo of a heart-shaped cermet.

system composed of a Ni-based superalloy and Al_2O_3, we show that our UHS approach can achieve highly dense microstructure (relative density is 94.3%), minimal loss of nickel component (1.80 wt %), and uniform grain size distribution (~2–6 μm). The high materials quality leads to good mechanical properties and

high temperature oxidation resistance (only 1.30 mg cm^{-2} weight increase after 100 h at 1,100°C in air). Our approach is scalable for larger samples (34 × 9 × 1 mm) and suitable for different shapes (e.g., star, heart, and bone shapes), as well as applicable to a range of cermet compositions and mass production. Beyond cermets, this approach can be extended to sinter a range of composite materials where the large physiochemical property differences of various components and phases are challenging to be tailored by conventional sintering methods. This study offers a new route toward sintering composite materials in a scalable, efficient, and high-quality manner.

EXPERIMENTAL PROCEDURES

Resource availability

Lead contact

Further information and requests for resources and materials should be directed to and will be fulfilled by the lead contact, Liangbing Hu (binghu@umd.edu).

Materials availability

All materials generated in this study will be made available on reasonable request.

Data and code availability

All data and code associated with the study have not been deposited in a public repository, but are available from the lead contact upon reasonable request.

Fabrication of the Ni-based superalloy and oxide cermets by ultrafast sintering

The raw materials of the Ni-based superalloy and oxides (Al_2O_3, ZrO_2, and YSZ) powders were mixed by ball milling in isopropanol for 12 h or simply by grinding. The Ni-based superalloy powder (~10 μm) was made at Carpenter Powder Products (Bridgeville, PA, USA) via the argon atomization process that is widely used to make metal powders for additive manufacturing. The nominal composition of this Ni-based superalloy is: 7.5Cr, 3.0Co, 4.0W, 5.5Ta, 7.5Al, 0.15Hf, and Ni-balance (all in weight percent). The mixed powders were pressed into pellets with dies and then directly sintered into cermets using an ultrafast sintering technique between two Joule-heating carbon felt strips in an Ar-filled glovebox for about 15 s. A STARPOWER power source was used as the DC power supply with tunable current (0–50 A) and voltage (0–50 V). The heating rate and temperature of the heater were precisely controlled by tuning the voltage (~40–50 V) of the DC power. The temperature of the heater was calculated from the UV-vis spectra measured using a Vision Research Phantom Miro M110 high-speed camera with an error of ±100 K.[28]

Preparation of Ni-based superalloy and Al_2O_3 cermet with a traditional furnace

The traditional sintering process was conducted using a furnace. A covered graphite crucible was used to place green pellets during sintering to provide a reductive environment. The sintered Ni-based superalloy and Al_2O_3 cermet was prepared at 1,500°C for 1 h.

Structure and composition characterizations

Microstructures and EDS mapping for the Ni-based superalloy and oxides cermets were characterized using an Hitachi SU-70 SEM. XRD patterns were obtained using a Bruker D8 Advance diffractometer and scanned between 10° and 80° using Cu Kα radiation. EBSD analysis was carried out using an FEI Scios Dual-Beam System. Ni contents were tested using an ICPE-9000 Atomic Emission Spectrometer.

Relative density tests

The relative density of each cermet is calculated by the ratio of actual density and theoretical density. The theoretical density of the cermet was calculated by formula to be:

$$\rho_{theoretical} = \frac{m_1 + m_2}{\frac{m_1}{\rho_1} + \frac{m_2}{\rho_2}}, \quad \text{(Equation 1)}$$

where m_1, m_2 are the weights of the Ni-based superalloy and Al_2O_3 in the mixed powder precursor, ρ_1, ρ_2 are the theoretical densities of Ni-based superalloy and Al_2O_3. The theoretical density of Ni-based superalloy was calculated by Thermo-Calc software and TCNI11 database, to be 8.29 g cm^{-3}. The theoretical density of Al_2O_3 is 3.95 g cm^{-3}. Then the calculated theoretical density of the cermet is 4.95 g cm^{-3}. The actual density of cermet was determined by the ratio of weight and volume of the cermet pellets. The actual densities of UHS and traditionally sintered Ni-based superalloy and Al_2O_3 cermet are 4.67 and 3.78 g cm^{-3}.

Mechanical properties tests

The three-point bending and compressive tests were conducted on an Instron 5565 universal tester. The support span and crosshead speed for three-point bending test are 26 mm and 1 mm min^{-1}, respectively. At least five samples were used to determine the bending and compressive strengths. The Vickers microhardness was determined using a digital Vickers hardness tester (model: Leco LM-800) under a load of 2 kg for 10 s. The average Vickers hardness value was obtained from five different regions of the cermet with four indentations made on each region. The fracture toughness was achieved by the Vickers indentation fracture technique using the formula proposed by Niihara et al.[29]

High-temperature stability test

High-temperature stability test was conducted in a 21100 Tube Furnace (Barnstead/Thermolyne) at 1,100°C continuously for 100 h in air. The sample used for the high-temperature stability test was a pellet with a diameter of 7.4 mm and thickness of 0.8 mm.

SUPPLEMENTAL INFORMATION

Supplemental information can be found online at https://doi.org/10.1016/j.matt.2021.11.008.

ACKNOWLEDGMENTS

The authors acknowledge the Maryland NanoCenter, Advanced Imaging and Microscopy (AIM) Lab, and X-ray Crystallographic Center. This work was supported by the Clark School Seed project and the Minta Martin Professorship fund.

AUTHOR CONTRIBUTIONS

M.G. and Q.D. contributed equally to this work. L. Hu, J.-C.Z., M.G., and Q.D. designed the experiments. M.G. synthesized the materials and conducted most of the characterizations. M.G. and Q.D. analyzed the results. H.X. and C.W. assisted in the sintering experiments. Y.Z., Y.W., and W.X. conducted the EBSD and hardness tests and analysis. X.W. performed the temperature measurement. W.Z. conducted the high-temperature oxidation resistance test. Z.L. and S.H. assisted in the mechanical tests. R.W. assisted in the SEM and XRD characterizations. L. Hao calculated the theoretical density of the cermet. G.C. assisted in temperature data analysis. M.G.,

Q.D., and L. Hu collectively wrote the paper. All authors commented on the final manuscript.

DECLARATION OF INTERESTS

The authors declare no competing interests.

Received: July 27, 2021
Revised: October 1, 2021
Accepted: November 3, 2021
Published: November 30, 2021

REFERENCES

1. Bewlay, B., Jackson, M.J., Zhao, J.-C., Subramanian, P.R., Mendiratta, M., and Lewandowski, J. (2003). Ultrahigh-temperature Nb-silicide-based composites. MRS Bull. *28*, 646–653.

2. Gild, J., Zhang, Y., Harrington, T., Jiang, S., Hu, T., Quinn, M.C., Mellor, W.M., Zhou, N., Vecchio, K., and Luo, J. (2016). High-entropy metal diborides: a new class of high-entropy materials and a new type of ultrahigh temperature ceramics. Sci. Rep. *6*, 1–10.

3. Perepezko, J.H. (2009). The hotter the engine, the better. Science *326*, 1068–1069.

4. Lo, K.-C., Chang, Y.-J., Murakami, H., Yeh, J.-W., and Yeh, A.-C. (2019). An oxidation resistant refractory high entropy alloy protected by $CrTaO_4$-based oxide. Sci. Rep. *9*, 1–12.

5. Zhao, J.-C., and Westbrook, J.H. (2003). Ultrahigh-temperature materials for jet engines. MRS Bull. *28*, 622–630.

6. Fahrenholtz, W.G., Ellerby, D.T., and Loehman, R.E. (2000). Al_2O_3-Ni composites with high strength and fracture toughness. J. Am. Ceram. Soc. *83*, 1279–1280.

7. Miazga, A., Konopka, K., Gizowska, M., and Szafran, M. (2014). Preparation of Al_2O_3-Ni cermet composites by aqueous gelcasting. Powder Metall. Met. Ceram. *52*, 567–571.

8. Aramian, A., Razavi, S.M.J., Sadeghian, Z., and Berto, F. (2020). A review of additive manufacturing of cermets. Addit. Manuf. *33*, 101130.

9. Ferraro, C., Meille, S., Réthoré, J., Ni, N., Chevalier, J., and Saiz, E. (2018). Strong and tough metal/ceramic micro-laminates. Acta Mater. *144*, 202–215.

10. Zhang, Y., Cheng, Y., Hu, H., and Yin, Z. (2017). Experimental study on cutting performance of microwave sintered Ti (C,N)/Al_2O_3 cermet tool in the dry machining of hardened steel. Int. J. Adv. Manuf. Tech. *91*, 3933–3941.

11. Russo, C.J., Harmer, M.P., Chan, H.M., and Miller, G.A. (1992). Design of a laminated ceramic composite for improved strength and toughness. J. Am. Ceram. Soc. *75*, 3396–3400.

12. Cho, J., Wang, C.M., Chan, H.M., Rickman, J.M., and Harmer, M.P. (1999). Role of segregating dopants on the improved creep resistance of aluminum oxide. Acta Mater. *47*, 4197–4207.

13. Wang, H., Singh, R., and Lowden, R. (1997). Thermal shock behaviour of unidirectional, 0°/90°, and 2-D woven fibre-reinforced CVI SiC matrix composites. J. Mater. Sci. *32*, 3305–3313.

14. Wang, C., Ping, W., Bai, Q., Cui, H., Hensleigh, R., Wang, R., Brozena, A.H., Xu, Z., Dai, J., Pei, Y., et al. (2020). A general method to synthesize and sinter bulk ceramics in seconds. Science *368*, 521–526.

15. Wang, C., Zhong, W., Ping, W., Lin, Z., Wang, R., Dai, J., et al. (2021). Rapid synthesis and sintering of metals from powders. Adv. Sci. *8*, 202004229.

16. Liu, H., Lu, H., Chen, D., Wang, H., Xu, H., and Zhang, R. (2009). Preparation and properties of glass-ceramics derived from blast-furnace slag by a ceramic-sintering process. Ceram. Int. *35*, 3181–3184.

17. Mahajan, S., Thakur, O.P., Bhattacharya, D.K., and Sreenivas, K. (2009). Study of structural and electrical properties of conventional furnace and microwave-sintered $BaZr_{0.10}Ti_{0.90}O_3$ ceramics. J. Am. Ceram. Soc. *92*, 416–423.

18. Chen, C.-h., Feng, K.-q., Zhou, Y., and Zhou, H.-l. (2017). Effect of sintering temperature on the microstructure and properties of foamed glass-ceramics prepared from high-titanium blast furnace slag and waste glass. Inter. J. Miner. Metall. Mater. *24*, 931–936.

19. Long, H., Mao, S., Liu, Y., Zhang, Z., and Han, X. (2018). Microstructural and compositional design of Ni-based single crystalline superalloys—a review. J. Alloys Compd. *743*, 203–220.

20. Wang, R.-H., Wang, X.-Q., Song, J.-G., Xu, M.-H., Li, Y.-Q., Liu, J.-Q., et al. (2017). Effect of sintering temperature on properties of Al_2O_3/Al cermets. Mater. Sci. Eng. 494–499. https://doi.org/10.1142/9789813226517_0072.

21. Gu, T., and Lu, H. (2011). Microwave sintering of Al_2O_3-ZrO_2-WC-Co cermets. J. Wuhan Univ. Technol. Mater. Sci. Ed. *26*, 289–291.

22. Kou, H.M., Pan, Y.B., and Guo, J.K. (2007). Microstructures and mechanical properties of Al/Al_2O_3 cermet composites reinforced by Al/Al_2O_3 core-shell particles. Adv. Mat. Res. *15*, 240–245.

23. Raimundo, R.A., Santos, K.V., Lourenço, C.S., Costa, F.A., Morales, M.A., Macedo, D.A., Silva, A.G., and Gomes, U.U. (2021). Effect of high energy milling on microstructure and mechanical properties of Al_2O_3-10 wt% Co composites consolidated by spark plasma sintering (SPS). Ceram. Int. *47*, 677–685.

24. Shi, G., Wang, Z., Liu, L., and Wang, C. (2015). Influence of Y_2O_3 addition on the Ti/Al_2O_3 cermets by hot pressing sintering. J. Alloys Compd. *628*, 413–415.

25. Verma, V., and Kumar, B.M. (2017). Synthesis, microstructure and mechanical properties of Al_2O_3/ZrO_2/CeO_2 composites with addition of nickel and titania processed by conventional sintering. Mater. Today Proc. *4*, 3062–3071.

26. Wu, C., Wang, Z., Li, Q., Shi, G., Liu, M., and Li, Y. (2014). Mechanical properties and microstructure evolution of Ti/Al_2O_3 cermet composite with CeO_2 addition. J. Alloys Compd. *617*, 729–733.

27. Yan, Q., Huang, Z., Wang, G.Y., and Jiang, D. (2008). The effect of microstructure on toughness of Ni/Al_2O_3 composites prepared by spark plasma sintering. J. Alloys Compd. *461*, 436–439.

28. Jacob, R.J., Kline, D.J., and Zachariah, M.R. (2018). High speed 2-dimensional temperature measurements of nanothermite composites: probing thermal vs. gas generation effects. J. Appl. Phys. *123*, 115902.

29. Niihara, K., Morena, R., and Hasselman, D. (1982). Evaluation of K_{Ic} of brittle solids by the indentation method with low crack-to-indent ratios. J. Mater. Sci. Lett. *1*, 13–16.